Proceedings Paper:
Candan, F. orcid.org/0000-0002-0803-610X, Beke, A., Shen, C. et al. (1 more author) (2022) An interacting multiple model correntropy Kalman filter approach for unmanned aerial vehicle localisation. In: Proceedings of the 2022 International Conference on INnovations in Intelligent SysTems and Applications (INISTA). 2022 International Conference on INnovations in Intelligent SysTems and Applications (INISTA), 08-12 Aug 2022, Biarritz, France. Institute of Electrical and Electronics Engineers . ISBN 9781665498111

https://doi.org/10.1109/INISTA55318.2022.9894214

An Interacting Multiple Model Correntropy Kalman Filter Approach for Unmanned Aerial Vehicle Localisation

1st Fethi Candan
Department of Automatic Control and Systems Engineering
University of Sheffield, Sheffield, S1 3JD, United Kingdom
fcandan1@sheffield.ac.uk

2nd Aykut Beke
Department of Control Systems Design
ASELSAN, Ankara, 06750, Turkiye
abeke@aselsan.com.tr

3rd Chen Shen
School of Information and Electronic Engineering
(Sussex Artificial Intelligence Institute)
Zhejiang Gongshang University, 310018, China
write2shen@sina.com

4th Lyudmila Mihaylova
Department of Automatic Control and Systems Engineering
University of Sheffield, Sheffield, S1 3JD, United Kingdom
l.s.mihaylova@sheffield.ac.uk

***Abstract*—This paper compares a conventional interacting multiple model Kalman filter (IMM-KF) filter and an interacting multiple models with maximum correntropy Kalman filter (IMM-MCKF). A nonlinear UAV dynamics model was used to compare these two methods. The compared filters estimated the position of the UAV under the noise distribution. Although KF has reliable accuracy, MCKF has got better results under non-Gaussian or mixed distributions. At this point, these filters have been investigated under maneuver and non-maneuver motion, and it is known that better advantages will be shown when both filters are used in the IMM. These filters have been compared under non-Gaussian distributions, and the Student's-T distribution has been selected as a non-Gaussian type. The performance validation and testing stages are carried out with variable degrees of freedom, and scaling matrix factors for the Student's-T distributions have been used. Results from simulation tests from 3000 independent Monte-Carlo runs are presented. In these experiments, UAV models and UAV trajectory results have been used.**

***Index Terms*—Multi-model approach, interacting multiple model, maximum correntropy Kalman filter, unmanned air vehicles**

I. INTRODUCTION

Nowadays, unmanned vehicle systems have been more interesting subjects for researchers. Especially unmanned air vehicles (UAVs) and unmanned ground vehicles (UGVs) have solved many important problems such as surveillance, military problem, observation, and rescue operations. However, controlling and position problems still have continued on UAVs to be resolved. Many linear and nonlinear controllers have been implemented to guarantee UAV stability. Linear quadratic regulator (LQR) [2], model predictive control (MPC) [25], proportional integral derivative (PID) [6] and Fuzzy PID (FPID) [7] are the most usage for UAVs.

Finding or localizing of UAV position has been another problem like controlling. In literature, there are several methods to accurately converge to exact positions like Kalman filter (KF), maximum correntropy Kalman filter (MCKF) [8], [21]. In the position of UAV, sensor fusion methods have been applied to IMU and GPS sensor data. An essential part of this application is identifying the correct model. However, the UAV states change drastically whether it follows a maneuvering or non-maneuvering trajectory. In this situation, interacting multiple model (IMM) approaches help to solve this problem.

In literature, there are several IMM methods have been deeply explained [3]–[5], [9], [10], [12]–[20], [22]–[24]. In ref [18], a survey paper has been written about maneuver and non-maneuver models for a system. The conventional IMM affects the measurement to set information updates with active models. The problem is model faults. If conventional IMM uses for fault-prognostic applications, it is faced with misleading state estimation. To overcome this problem, Fuzzy and IMM structures have been merged to detect fault-tolerant in ref [9]. It is seen that defining dynamical models have played an important role in the application. For this reason, in ref [18], different dynamical models for maneuvering target tracking have been researched. Moreover, the cubature Kalman filter implemented IMM approach has been used for nonlinear systems in ref [20], and this approach has been tested on maneuvering target tracking to represent the switching probability; the approach employs a Markov process. Another research has shown different filtering for Markovian switching: interacting multiple model particle filtering in ref [5]. Considering the conventional filter, it can look the same as each other. However, the particle filter affects the mixture of Gaussian probability densities. That means that it is able to manage non-linearities in the system and non-Gaussian noise [15], [16].

978-1-6654-9810-4/22/$31.00

As can be seen that there are several advantages of IMM approaches for different applications. In this paper, Interacting multiple model merged with maximum correntropy Kalman filter (IMM-MCKF) has been proposed for UAV position estimation. In ref [8], [10], [21], MCKF performance has been compared with conventional method under Gaussian and non-Gaussian distributions.

This paper is organized as follows. Section II describes the methods of the UAV model and interacting multiple model. The next section is about proposed IMM with maximum correntropy Kalman filter. Simulation results are given in Section IV. The last section presents the conclusion and future work.

II. METHODOLOGY

This section presents Crazyflie 2.0 dynamic model [1], controller and sensor estimation method proposed in this paper. After explaining the dynamical model and control of Crazyflie 2.0, IMM and MCKF have been explained with formulations and structures.

A. Dynamical Modelling and Control of Crazyflie 2.0

In this paper, the Crazyflie 2.0 UAV [1] linear dynamic model has been used and the velocity controller has been designed for this system as in [7]. Fig. 1 shows the body frame of UAV is fixed to the Center of Mass (CoM). position of UAV is defined as $\zeta^I = [x\,y\,z]^T$ and orientation of the body frame relative to the inertial frame is given by $\eta = [\phi\ \theta\ \psi]^T$, roll, pitch, yaw Euler angles, respectively, and also R is the rotation matrix between frame I and B [7], [11].

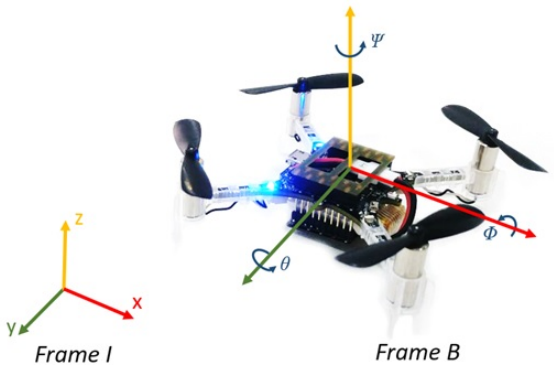

Fig. 1. Crazyflie 2.0 UAV frame

$$\begin{aligned} \upsilon^I &= \dot{\zeta}^I = R\upsilon^B \\ \omega^I &= \dot{\eta}^I = T\omega^B \end{aligned} \tag{1}$$

(1) where the transformation matrix ($\mathbf{T}$) is given by:

$$\mathbf{T} = \begin{bmatrix} 1 & s(\phi)t(\theta) & c(\phi)t(\theta) \\ 0 & c(\phi) & -s(\phi) \\ 0 & s(\phi)/c(\theta) & c(\phi)/c(\theta) \end{bmatrix} \tag{2}$$

with s(.), c(.), and t(.) are abbreviated from sine, cosine and tangent functions, respectively.

The dynamics of the UAV can be shown with using the Newton-Euler formulation as follows:

$$\begin{aligned} m\dot{\upsilon}^I &= F^I = F^I_{gravity} + F^I_{thrust} \\ I_B\dot{\omega}^B &= -\omega^B \times \tau^B_{rotor} \end{aligned} \tag{3}$$

In the Eq. (3) shown, m is the mass of the UAV, I_B is the inertia matrix for center of UAV's mass (CoM). F^I give external forces of system and with this forces, torques $\tau_{rotor} = \begin{bmatrix}\tau\phi & \tau\theta & \tau\psi\end{bmatrix}$ can be applied by rotors. These external forces are also include gravity force which is implemented vertically of CoM is given as:

$$\begin{aligned} F^I_{gravity} &= \begin{bmatrix}0 & 0 & -mg\end{bmatrix}^T \\ F^I_{thrust} &= RF^B_{gravity} \end{aligned} \tag{4}$$

Considering UAV's body frame, the forces are existed of propellers:

$$F^B_{thrust} = \begin{bmatrix}0 & 0 & b\sum_{i=1}^{4}\Omega_i^2\end{bmatrix}^T \tag{5}$$

In the above Eqn. (5), there is shown thrust coefficient (b) and angular velocity of rotor (Ω_i). In Eqn. (6). l is the distance between the UAV's CoM. Lastly, the dynamical equations of motion is written:

$$\dot{\upsilon}^B = \begin{bmatrix}\ddot{x}\\ \ddot{y}\\ \ddot{z}\end{bmatrix} = \tfrac{b}{m}\sum_{i=1}^{4}\Omega_i^2 = \begin{bmatrix} s\phi s\psi + c\phi s\theta c\psi \\ -s\phi c\theta + c\phi s\theta s\psi \\ c\phi c\theta \end{bmatrix} - \begin{bmatrix}0\\0\\g\end{bmatrix}$$

$$\dot{\omega}^B = I_B^{-1}.\tau^B_{rotor} = \begin{bmatrix} \frac{1}{I_x}bl(\Omega_4^2 - \Omega_2^2) \\ \frac{1}{I_y}bl(\Omega_3^2 - \Omega_1^2) \\ \frac{1}{I_z}bl(\Omega_4^2 - \Omega_3^2 + \Omega_2^2 - \Omega_1^2)) \end{bmatrix} \tag{6}$$

In this paper we have focused on position and velocity estimation. For this result, position controller has been used. General discrete PID controller formula can be seen in Eqn. (7). PID parameters are $P = 0.034$, $I = 6.3e-06$ and $D = 0.083$, respectively. Sampling time (T_s) has been chosen 0.01s. Parameters have been found by using genetic algorithm which is a type of optimization methods.

$$u_t = e_t\left[K_p + \tfrac{K_i}{1-z^{-1}} + K_d(1-z^{-1})\right] \tag{7}$$

B. Interacting Multiple Model

The Interacting Multiple Model (IMM) is a type of hybrid state estimation algorithm for Markovian linear systems. It has many advantages in terms of computation time, target tracking, fault detection and classify the models [19]. The model structure has been illustrated in Fig. 2. Each model has different probability weight. Then, IMM calculate estimate and covariance matrices to send to Kalman filter as inputs [19]. In this section, general IMM formula parts have been explained.

There are three models have been implemented in proposed IMM structure. They have been one constant velocity ($\mathbf{F}_{CVM}$) and two different constant turning models ($\mathbf{F}_{CTM}$).

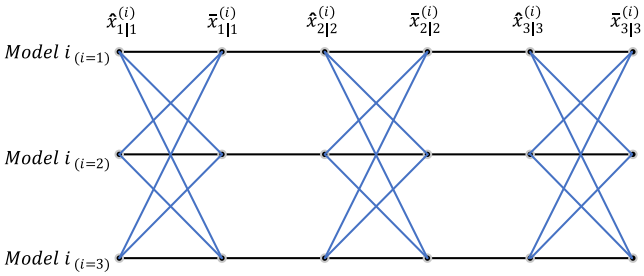

Fig. 2. Interacting multiple model structure [19]

$$\mathbf{F}_{CVM} = \begin{bmatrix} 1 & \mathrm{T} & 0 & 0 \\ 0 & 1 & 0 & 0 \\ 0 & 0 & 1 & \mathrm{T} \\ 0 & 0 & 0 & 1 \end{bmatrix} \tag{8}$$

$$\mathbf{F}_{CTM} = \begin{bmatrix} 1 & sin(\omega_i \mathrm{T})/\omega_i & 0 & -(1-cos(\omega_i \mathrm{T})/\omega_i \\ 0 & cos(\omega_i \mathrm{T}) & 0 & -sin(\omega_i \mathrm{T}) \\ 0 & (1-cos(\omega_i \mathrm{T}))/\omega_i & 1 & sin(\omega_i \mathrm{T})/\omega_i \\ 0 & sin(\omega_i \mathrm{T}) & 0 & cos(\omega_i \mathrm{T}) \end{bmatrix} \tag{9}$$

In Eqn. (8) and (9), sampling time is declared as T and maneuverings of UAV ω have existed of 2 parts. For the left acceleration model, ω_i is $\omega = 2\pi/180$, on the other hand $\omega = -2\pi/180$ is chosen for right acceleration model. These two acceleration models generate constant turning model($\mathbf{F}_{CTM}$).

The IMM consists of 4 parts; mixing, filtering, mode update, and output, respectively. Predicted model probability and mixing weight, estimate and covariance are in the mixing part.

Firstly, predicted model probability ($\hat{\mu}^{(i)}_{k|k-1}$) formula Eqn. (10), and mixing weight ($\mu^{j|i}_{k-1}$) can be seen in Eqn. (11). Here z^k shows current measurement data.

$$\hat{\mu}^{(i)}_{k|k-1} = \boldsymbol{P}\left\{m^{(i)}_k | z^{k-1}\right\} = \textstyle\sum_j \pi_{ji} \hat{\mu}^{(j)}_{k-1} \tag{10}$$

$$\mu^{j|i}_{k-1} = \boldsymbol{P}\left\{m^{(j)}_{k-1} | m^{(i)}_k, z^{k-1}\right\} = \pi_{ji}\mu^{(j)}_{k-1}/\hat{\mu}^{(i)}_{k|k-1} \tag{11}$$

After that, estimated state Eqn. (12) and covariance Eqn. (13) and can be calculated:

$$\bar{x}^{(i)}_{k-1|k-1} = E\left[x_{k-1} | m^{(i)}_k, z^{k-1}\right] = \textstyle\sum_j \hat{x}^{(j)}_{k-1|k-1}\mu^{j|i}_{k-1} \tag{12}$$

$$\bar{\boldsymbol{P}}^{(i)}_{k-1|k-1} = \textstyle\sum_j \left[P^{(j)}_{k-1|k-1} + \left(\bar{x}^{(i)}_{k-1|k-1} - \hat{x}^{(j)}_{k-1|k-1}\right) \left(\bar{x}^{(i)}_{k-1|k-1} - \hat{x}^{(j)}_{k-1|k-1}\right)'\right] \mu^{j|i}_{k-1} \tag{13}$$

These mixed-estimated state and covariance matrices has been used for proposed Kalman filter. Next section Maximum correntropy Kalman filter (MCKF) will be explained. In this section, it is assumed that the Kalman filter is applied. Also, Kalman filter outputs has been defined as updated state $\hat{x}^{(i)}_{k|k}$ and updated covariance $\boldsymbol{P}^{(i)}_{k|k}$.

After skipping filtering part, model probability update part has been used. It means that model likelihood and model probability will be calculated.

The model likelihood and the model probability are given Eqn. (14) and Eqn. (15), respectively.

$$L^{(i)}_k = \boldsymbol{p}\left[\tilde{z}^{(i)}_k | m^{(i)}_k, z^{k-1}\right] \cong \frac{e^{-(1/2)(\tilde{z}^{(i)}_k)'(S^i_k)^{-1}(\tilde{z}^{(i)}_k)}}{\sqrt{|2\pi S^i_k|}} \tag{14}$$

$$\mu^i_k = \boldsymbol{P}\left[m^{(i)}_k | z^k\right] = \frac{\hat{\mu}^{(i)}_{k|k-1}L^{(i)}_k}{\sum_j \hat{\mu}^j_{k|k-1}L^{(j)}_k} \tag{15}$$

The last part of the IMM is described next. It is composed of the overall state estimate and the covariance matrix.

$$\hat{x}_{k|k} = E\left[x_k | z^k\right] = \textstyle\sum_i \hat{x}^{(i)}_{k|k}\mu^{(i)}_k \tag{16}$$

$$\boldsymbol{P}_{k|k} = \textstyle\sum_i \left[\boldsymbol{P}^{(i)}_{k|k} + \left(\hat{x}_{k|k} - \hat{x}^i_{k|k}\right)\left(\hat{x}_{k|k} - \hat{x}^i_{k|k}\right)'\right]\mu^{(i)}_k. \tag{17}$$

The following Section III presents the developed IMM-MCKF algorithm.

III. Proposed IMM Approach with MCKF

The Maximum Correntropy Kalman filter (MCKF) is based on maximum correntropy criteria and a fixed-point iterative algorithm [8], [10], [21]. It is well known that the conventional Kalman filter gives a good result under Gaussian noises. However, its performance worsens under non-Gaussian noises. It is an inevitable consequence due to the use of the traditional Kalman filter based on the Gaussian distribution [8], [10], [21].

Before starting the whole algorithm, correntropy criteria will be explained. When given two random variables $X, Y \in \mathbb{R}$ with joint distributed function $d\mathbf{F}_{XY}(xy)$, correntropy is described by

$$V(X,Y) = E\left[\kappa(X,Y)\right] = \int \kappa(x,y) d\mathbf{F}_{XY}(xy) \tag{18}$$

In Eqn. 18, shift-invariant Mercer Kernel is indicated as $\kappa(.,.)$ and E shows the expectation operator. In this paper, Gaussian Kernel has been chosen and it is given by

$$\kappa(x,y) = \mathrm{G}_\sigma(\epsilon) = \mathrm{e}^{\left(-\frac{\epsilon^2}{2\sigma^2}\right)}. \tag{19}$$

where $\mathrm{e} = x - y$ is calculated. Moreover, the σ value is chosen to be equal to 7 and the kernel bandwidth ε gets 10^{-3} values.

For state prediction and covariance matrix prediction can be performed with the following equations:

$$\begin{aligned} \hat{\mathbf{x}}(k|k-1) &= \mathbf{F}(k-1)\hat{\mathbf{x}}(k-1|k-1) \\ \mathbf{P}(k|k-1) &= \mathbf{F}(k-1)\mathbf{P}(k-1|k-1)\mathbf{F}^T(k-1) + \mathbf{Q}(k-1). \end{aligned} \tag{20}$$

The kernel bandwidth σ and small positive threshold ε are set up accordingly, from practical considerations. Also,

$$\begin{bmatrix} \mathbf{P}(k|k-1|) & 0 \\ 0 & \mathbf{R}(k) \end{bmatrix}$$

$$= \begin{bmatrix} \mathbf{P}_p(k|k-1|)\mathbf{P}_p^T(k|k-1|) & 0 \\ 0 & \mathbf{B}_r(k)\mathbf{B}_r^T(k) \end{bmatrix} \tag{21}$$

$$= \mathbf{B}(k)\mathbf{B}^T(k).$$

In Eqn. 21, $\mathbf{B}(k)$ has existed of Cholesky decomposition. Then,

$$\mathbf{D}(k) = \mathbf{W}(k)\mathbf{x}(k) + \mathbf{e}(k)$$

$$\mathbf{D}(k) = \mathbf{B}^{-1}(k)\begin{bmatrix} \hat{\mathbf{x}}(k|k-1|) \\ \mathbf{y}(k) \end{bmatrix}, \quad \mathbf{W}(k) = \mathbf{B}^{-1}(k)\begin{bmatrix} \mathbf{I} \\ \mathbf{H}(k) \end{bmatrix} \tag{22}$$

For the posterior estimation, it is updated by using fixed-point iteration for each $\hat{\mathbf{x}}^{(t)}(k|k)$

$$\hat{\mathbf{x}}^{(t)}(k|k) = \hat{\mathbf{x}}(k|k-1) + \widetilde{\mathbf{K}}^{(t-1)}(\mathbf{y}(k) - \mathbf{H}(k)\hat{\mathbf{x}}(k|k-1)) \tag{23}$$

Considering the above equation, it includes some parameters which are detailed between in Eqn. 24 and Eqn. 29

$$\widetilde{\mathbf{K}}^{(t-1)}(k) = \widetilde{\mathbf{P}}^{(t-1)}(k|k-1|)\hat{\mathbf{H}}^{\mathrm{T}}(k)... \times \left(\mathbf{H}(k)\widetilde{\mathbf{P}}(k|k-1|)\mathbf{H}^{\mathrm{T}}(k) + \widetilde{\mathbf{R}}^{(t-1)}(k)\right)^{-1} \tag{24}$$

$$\widetilde{\mathbf{P}}^{(t-1)}(k|k-1) = \mathbf{B}_p(k|k-1)\left(\widetilde{\mathbf{C}}_x^{(t-1)}(k)\right)^{-1} ... \times \mathbf{B}_p^{\mathrm{T}}(k|k-1) \tag{25}$$

$$\widetilde{\mathbf{R}}^{(t-1)}(k) = \mathbf{B}_r(k)\left(\widetilde{\mathbf{C}}_y^{(t-1)}(k)\right)^{-1} \times \mathbf{B}_r^{\mathrm{T}}(k) \tag{26}$$

$$\widetilde{\mathbf{C}}_x^{(t-1)}(k) = \begin{bmatrix} \mathrm{G}_\sigma\left(\widetilde{e}_1^{(t-1)}(k)\right) & 0 & 0 \\ 0 & \ddots & 0 \\ 0 & 0 & \mathrm{G}_\sigma\left(\widetilde{e}_n^{(t-1)}(k)\right) \end{bmatrix} \tag{27}$$

$$\widetilde{\mathbf{C}}_y^{(t-1)}(k) = \begin{bmatrix} \ddots & 0 & 0 & 0 \\ 0 & \mathrm{G}_\sigma\left(\widetilde{e}_{n+1}^{(t-1)}(k)\right) & 0 & 0 \\ 0 & 0 & \ddots & 0 \\ 0 & 0 & 0 & \mathrm{G}_\sigma\left(\widetilde{e}_{n+m}^{(t-1)}(k)\right) \end{bmatrix} \tag{28}$$

$$\widetilde{e}_i^{(t-1)} = d_i(k) - \mathbf{w}_i(k)\hat{\mathbf{x}}^{(t-1)}(k|k) \tag{29}$$

In Eqn. (30), estimation states have been compared with the current and the last step by small positive threshold (ε).

$$\frac{\left\|\hat{\mathbf{x}}^{(t)}(k|k) - \hat{\mathbf{x}}^{(t-1)}(k|k)\right\|}{\left\|\hat{\mathbf{x}}^{(t-1)}(k|k)\right\|} \leq \varepsilon \tag{30}$$

When the required condition in the above equation is satisfied, posterior covariance matrix can be determined

$$\mathbf{P}(k|k) = \left(\mathbf{I} - \widetilde{\mathbf{K}}(k)\mathbf{H}(k)\right)\mathbf{P}(k|k-1)\left(\mathbf{I} - \widetilde{\mathbf{K}}(k)\mathbf{H}(k)\right)^{\mathrm{T}} + \widetilde{\mathbf{K}}(k)\mathbf{R}(k)\widetilde{\mathbf{K}}(k)^{\mathrm{T}} \tag{31}$$

In Fig. 3, the architecture of IMM-MCKF has been shown. In this paper, unlike the conventional IMM structure, IMM and MCKF have been combined each other. Compare with the proposed architecture, the conventional one has used traditional Kalman filter in the model-conditioned filtering part (IMM-KF or IMM). With the proposed method, it has been aimed to estimate localisation under non-uniform distribution. For this reason, Students-T distribution which is a type of non-uniform or non-Gaussian distribution has been used for the experiments.

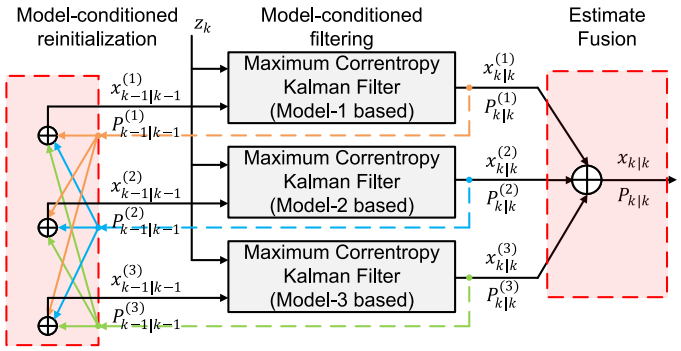

Fig. 3. Architecture of IMM-MCKF

At the end of this section, IMM and MCKF have been explained in terms of equations and structures. Simulation results will be given by the following section.

IV. SIMULATION RESULTS

This paper is about the implementation of IMM-MCKF for the UAV. Unlike conventional methods such as IMM-KF or single model approaches, IMM-MCKF has been tested under non-uniform distribution. In this way, Student's-T distribution has been used to choose different degrees of freedoms [15], [16], [24]. All experiments have been run 3000 independent Monte-Carlo times. The computer used for these experiments has an Intel i7 processor 16GB RAM Matlab 2021 environment.

For the experiments, the same error covariance matrices have been chosen. The covariance matrices have been defined as Gaussian covariances. Two different IMM methods have been compared under Student's-T distribution. Also, variable degrees of freedom (DoF) has been selected for the Student's-T distribution in these tests. These distributions have been used as noises for the UAV measurement.

In this paper, Student's T distributions have been chosen as a Non-Gaussian Distribution, and this noise has been added to measurement. In Eqn. (32), $\mathbf{H}$ measurement matrix has been defined as below:

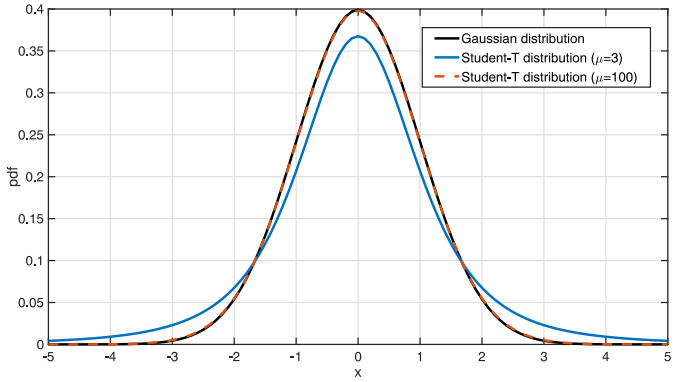

Fig. 4. Gaussian and Student's-T distributions

$$\mathbf{H} = \begin{bmatrix} 1 & 0 & 0 & 0 \\ 0 & 0 & 1 & 0 \end{bmatrix}. \tag{32}$$

It has been remarked that initial covariance, process noise, and measurement noise matrices have been constructed with the same values for a fair comparison of IMM filters.

In Fig. 4, Gaussian and Student's-T distributions have been shown. The important point of this figure has been about changing DoF. Noises have been implemented into measured data $(x, y, \upsilon_x, \upsilon_y)$ with using scaling matrix factor (β). The scaling matrix factor shows the power of noises.

In Fig. 5 shows UAV reference trajectory under Student's-T noises with choosing $\mu_1 = 4$ and $\mu_2 = 8$. Moreover, β has been chosen 0.02. Trajectory reference, noise added reference, IMM-KF result, and IMM-MCKF result has been shown with different colors as green, black, blue, and red, respectively.

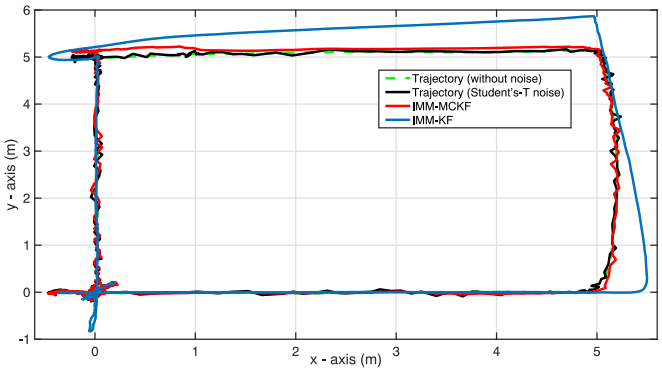

Fig. 5. Reference trajectory tracking under Student's-T distribution ($\mu_1 = 4$ and $\mu_2 = 8$)

It is shown that IMM-MCKF and IMM-KF have given almost the same results for the first x-axis. Then, IMM-MCKF has been shown better results than IMM-KF at the first y-axis and the second side of x-axis.

After the first experiment, $\mu_1 = 1$, $\mu_2 = 3$ and $\beta = 0.002$ have been selected for the second experiment. With these selections, DoF and scaling matrix factor effects have been seen in Fig.6. Considering the IMM-KF reference trajectory

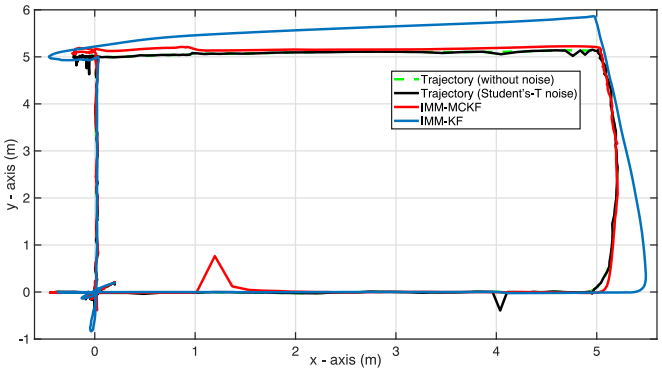

Fig. 6. Reference trajectory tracking under Student's-T distribution ($\mu_1 = 1$ and $\mu_2 = 3$)

estimation, the UAV has gone out of axes. Although, IMM-MCKF has been continued to reference with a small oscillation.

The testing parameters have been given in Table I. The average of Root Mean Square Errors (RMSEs) values (is meters) over the 3000 Monte Carlo independent runs and their total times (in seconds) have been given in this table. Considering the total time differences for both experiments, the IMM-KF has given a 3.35 times faster response.

TABLE I
TEST RESULTS OF IMM-KF AND IMM-MCKF

Multi-Models	**Student's-T Distribution**			
	$\mu = 4-8$ $\beta = 0.02$		$\mu = 1-3$ $\beta = 0.002$	
	Time	**RMSE**	**Time**	**RMSE**
IMM-MCKF	7710 sec	0.081 m	6950 sec	0.077
IMM-KF	2300 sec	0.335	2024 sec	0.343

Table I shows the average RMSE and the total computational time of both algorithms. When choosing $\mu_1 = 4$, $\mu_2 = 8$ and $\beta = 0.02$, the IMM-MCKF has been given 4.1 times better RMSE results than IMM-KF. These consequences have been almost the same with the second experiment. IMM-MCKF has been 4.45 times better than the other under non-Gaussian noises.

V. CONCLUSION AND FUTURE WORKS

This paper has shown how to estimate UAV states with an IMM-MCKF approach. Unlike conventional methods such as IMM-KF or single model approaches, IMM-MCKF has been tested under a non-uniform distribution. In this paper, the Student's-T distribution has been used. Simulation results showed that IMM-MCKF results are better than the IMM-KF in terms of RMSE. Furthermore, although the computational time is a challenge for the IMM-MCKF, the IMM-KF is faster. However, both algorithms could be applied in real-time systems after a further optimisation of the code efficiency. In this experiment, the computational time is averaged over 3000 repeated Monte Carlo runs and it is 3.3522 seconds for IMM-MCKF and 0.7667 seconds for the IMM-KF.

Future work will focus on a swarm of UAVs and control with the developed estimation approaches.

Acknowledgments. We acknowledge the Turkish government for funding the doctoral scholarship of Fethi Candan.

REFERENCES

[1] "Bitcraze, crazyflie," https://www.bitcraze.io/documentation/start, accessed: 2022-02-03.

[2] L. M. Argentim, W. C. Rezende, P. E. Santos, and R. A. Aguiar, "Pid, lqr and lqr-pid on a quadcopter platform," in *2013 International Conference on Informatics, Electronics and Vision (ICIEV)*. IEEE, 2013, pp. 1–6.

[3] W. Blanding, P. Willett, and Y. Bar-Shalom, "Ml-pda: Advances and a new multitarget approach," *EURASIP Journal on Advances in Signal Processing*, vol. 2008, pp. 1–13, 2007.

[4] H. A. Blom and Y. Bar-Shalom, "The interacting multiple model algorithm for systems with markovian switching coefficients," *IEEE transactions on Automatic Control*, vol. 33, no. 8, pp. 780–783, 1988.

[5] Y. Boers and J. N. Driessen, "Interacting multiple model particle filter," *IEE Proceedings-Radar, Sonar and Navigation*, vol. 150, no. 5, pp. 344–349, 2003.

[6] F. Candan, Y. Peng, and L. Mihaylova, "A comparison of obstacle dependant gaussian and hybrid potential field methods for collision avoidance in multi-agent systems," in *Proceedings of the 1st International Conference on Computing and Machine Intelligence (ICMI 2021)*. Sheffield, 2021.

[7] F. Candan, A. Beke, and T. Kumbasar, "Design and deployment of fuzzy PID controllers to the nano quadcopter Crazyflie 2.0," in *Proc. of the Innovations in Intelligent Systems and Applications (INISTA) Conf.* IEEE, 2018, pp. 1–6.

[8] B. Chen, X. Liu, H. Zhao, and J. C. Principe, "Maximum correntropy kalman filter," *Automatica*, vol. 76, pp. 70–77, 2017.

[9] L. B. Cosme, W. M. Caminhas, M. F. S. V. D'Angelo, and R. M. Palhares, "A novel fault-prognostic approach based on interacting multiple model filters and fuzzy systems," *IEEE Transactions on Industrial Electronics*, vol. 66, no. 1, pp. 519–528, 2018.

[10] X. Fan, G. Wang, J. Han, and Y. Wang, "Interacting multiple model based on maximum correntropy kalman filter," *IEEE Transactions on Circuits and Systems II: Express Briefs*, vol. 68, no. 8, pp. 3017–3021, 2021.

[11] M. Greiff, "Modelling and control of the crazyflie quadrotor for aggressive and autonomous flight by optical flow driven state estimation," 2017.

[12] B. A. Gunawan, Y. Liu, and X. Li, "Adaptive localisation for unmanned surface vehicles using imu-interacting multiple model," in *2020 International Conference on System Science and Engineering (ICSSE)*. IEEE, 2020, pp. 1–6.

[13] I. Hwang, C. E. Seah, and S. Lee, "A study on stability of the interacting multiple model algorithm," *IEEE Transactions on Automatic Control*, vol. 62, no. 2, pp. 901–906, 2016.

[14] M. Jafarinasab, S. Sirouspour, and E. Dyer, "Model-based motion control of a robotic manipulator with a flying multirotor base," *IEEE/ASME Transactions on Mechatronics*, vol. 24, no. 5, pp. 2328–2340, 2019.

[15] D. Li and J. Sun, "Robust interacting multiple model filter based on student's t-distribution for heavy-tailed measurement noises," *Sensors*, vol. 19, no. 22, p. 4830, 2019.

[16] Q. Li, Y. Ben, J. Tan, S. M. Naqvi, and J. Chambers, "Robust selection of the degrees of freedom in the student'st distribution through multiple model adaptive estimation," *Signal Processing*, vol. 153, pp. 255–265, 2018.

[17] X. R. Li and Y. Bar-Shalom, "A recursive multiple model approach to noise identification," *IEEE Transactions on Aerospace and Electronic Systems*, vol. 30, no. 3, pp. 671–684, 1994.

[18] X. R. Li and V. P. Jilkov, "Survey of maneuvering target tracking: dynamic models," in *Signal and Data Processing of Small Targets 2000*, vol. 4048. International Society for Optics and Photonics, 2000, pp. 212–235.

[19] X.-R. Li, Y. Bar-Shalom, and W. D. Blair, "Engineer's guide to variable-structure multiple-model estimation for tracking," *Multitarget-multisensor tracking: Applications and advances.*, vol. 3, pp. 499–567, 2000.

[20] H. Liu and W. Wu, "Interacting multiple model (imm) fifth-degree spherical simplex-radial cubature kalman filter for maneuvering target tracking," *Sensors*, vol. 17, no. 6, p. 1374, 2017.

[21] X. Liu, B. Chen, H. Zhao, J. Qin, and J. Cao, "Maximum correntropy kalman filter with state constraints," *IEEE Access*, vol. 5, pp. 25 846–25 853, 2017.

[22] E. Mazor, A. Averbuch, Y. Bar-Shalom, and J. Dayan, "Interacting multiple model methods in target tracking: a survey," *IEEE Transactions on aerospace and electronic systems*, vol. 34, no. 1, pp. 103–123, 1998.

[23] C. E. Seah and I. Hwang, "State estimation for stochastic linear hybrid systems with continuous-state-dependent transitions: an imm approach," *IEEE Transactions on Aerospace and Electronic Systems*, vol. 45, no. 1, pp. 376–392, 2009.

[24] C. Shen and L. Mihaylova, "A flexible robust student's t-based multi-model approach with maximum versoria criterion," *Signal Processing*, vol. 182, p. 107941, 2021.

[25] W. Zhao and T. H. Go, "Quadcopter formation flight control combining mpc and robust feedback linearization," *Journal of the Franklin Institute*, vol. 351, no. 3, pp. 1335–1355, 2014.